Journal of the Mechanical Behavior of Biomedical Materials 85 (2018) 109–116

Contents lists available at ScienceDirect

Journal of the Mechanical Behavior of Biomedical Materials

journal homepage: www.elsevier.com/locate/jmbbm

Comparison of five viscoelastic models for estimating viscoelastic parameters using ultrasound shear wave elastography

Boran Zhou, Xiaoming Zhang*

Department of Radiology, Mayo Clinic College of Medicine, 200 1st St SW, Rochester, MN 55905, USA

ARTICLE INFO

Keywords:
Ultrasound shear wave elastography (USVE)
Viscoelastic models
Fractional Voigt
Shear wave speed

ABSTRACT

The purpose of this study is to compare five viscoelastic models (Voigt, Maxwell, standard linear solid, spring-pot, and fractional Voigt models) for estimating viscoelastic properties based on ultrasound shear wave elastography measurements. We performed the forward problem analysis, the inverse problem analysis, and experiments. In the forward problem analysis, the shear wave speeds at different frequencies were calculated using the Voigt model for given shear elasticity and varying shear viscosity.

In the inverse problem analysis, the viscoelastic parameters were estimated from the given wave speeds for the five viscoelastic models using the least-square regression. The experiment was performed in a tissue-mimicking phantom. A local harmonic vibration was generated via a mechanical shaker on the phantom at five frequencies (100, 150, 200, 250, and 300 Hz) and an ultrasound transducer was used to capture the tissue motion. Shear wave speed of the phantom was measured using the ultrasound shear wave elastography technique. The parameters for different viscoelastic models for the phantom were identified. For both analytical and experimental studies, ratios of storage to loss modulus as a function of excitation frequency for different viscoelastic models were calculated. We found that the Voigt and fractional Voigt models fit well with the shear wave speed - frequency and ratio of storage to loss modulus – frequency relationships both in analytical and experimental studies.

1. Introduction

Systemic sclerosis (SSc), also known as scleroderma, is a multi-organ connective tissue disease manifested by immune dysregulation and organ fibrosis. Fibrosis can be taken as one of the most important factors of the SSc. Fibrosis occurs not only in skin but also in the lung, heart, tendons, and within the perivascular tissue (Kubo et al., 2017; Prim et al., 2016; Shazly et al., 2015; Zhang et al., 2018a). So far, elasticity of skin in patients affected by SSc is evaluated using the modified Rodnan skin score or using a durometer to measure skin hardness (Clements et al., 1995). Yet, they are user-dependent and less sensitive to many less dramatic skin changes and difficult to quantify over short intervals if the treatments are beneficial to patients. There is a pressing need for more accurate and sensitive quantification to monitor therapeutic responses or progression of disease over time.

Recently, ultrasound shear wave elastography (USWE) has been applied to assess skin and lung diseases (Cheng et al., 2018; Osborn et al., 2017; Zhang et al., 2017b). USWE seeks to investigate the viscoelastic properties within the region of interest that will affect the shear wave motion, which is related to changes in the viscoelastic properties of the soft tissue altered by various pathologies (Zhang et al., 2018b). This technique is independent of both excitation and detection probes. It measures the speed and decay of the wave propagation on the skin. Our technique has the potential for the early diagnosis of scleroderma, evaluation of the progression, and response to treatments in the routine clinical care setting.

The appropriate form of a viscoelastic model for soft biological tissues, especially for SSc, is still a subject of much research, particularly in ultrasound elastography. Various viscoelastic constitutive models, which attempt to correlate experimental measurements with frequency-dependent material viscoelasticity, have been proposed to interpret shear wave measurements. The Voigt model of viscoelasticity has been used to accurately capture dynamic behavior of soft biological tissues (Royston et al., 2011). The standard linear solid (SLS) model consists of a parallel combination of a Maxwell element (spring and dashpot in series) with a spring (Leng et al., 2018). A spring-pot model, as an alternative of increasing the number of components of the constitutive model, consists of a frequency-independent shear modulus μ and a dimensionless structure geometry parameter α (Asbach et al., 2010). The fractional order viscoelastic model, for which material is

* Corresponding author.
E-mail address: Zhang.xiaoming@mayo.edu (X. Zhang).

https://doi.org/10.1016/j.jmbbm.2018.05.041
Received 3 April 2018; Received in revised form 9 May 2018; Accepted 29 May 2018
Available online 30 May 2018

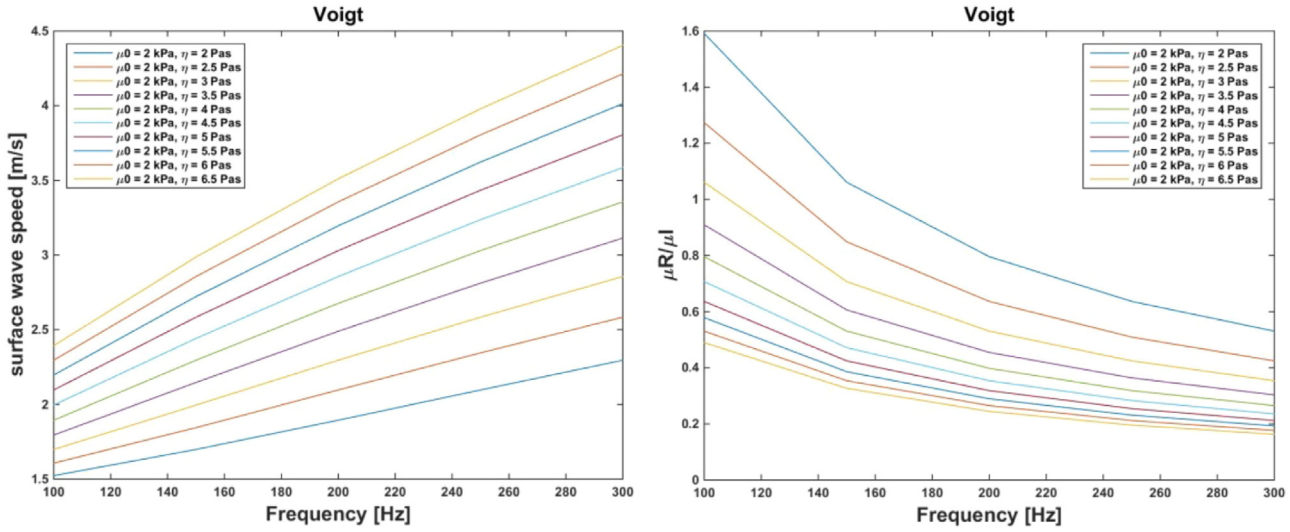

Fig. 1. Shear wave speed and ratio of storage to loss modulus of Voigt models of various material parameters at different excitation frequencies.

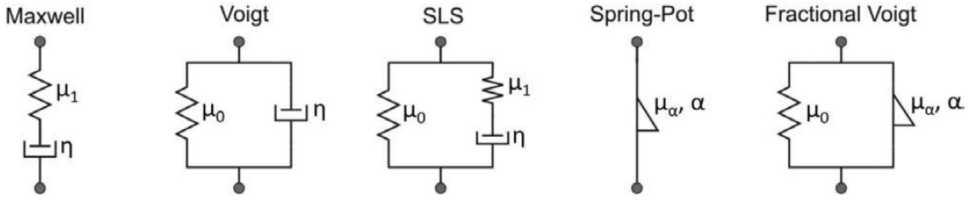

Fig. 2. Viscoelastic models used for this study.

Table 1
Storage and loss moduli of selected viscoelastic models. η is the shear viscosity and α is the fractional exponent.

Viscoelastic Model	Storage Modulus μ_R	Loss Modulus μ_I
Maxwell	$\frac{\omega^2\eta^2\mu_1}{\mu_1^2+\omega^2\eta^2}$	$\frac{\omega\eta\mu_1^2}{\mu_1^2+\omega^2\eta^2}$
Voigt	μ_0	$\omega\eta$
SLS	$\frac{\mu_0\mu_1^2+\omega^2\eta^2(\mu_0+\mu_1)}{\mu_1^2+\omega^2\eta^2}$	$\frac{\omega\eta\mu_1^2}{\mu_1^2+\omega^2\eta^2}$
Spring-pot	$\mu_\alpha\omega^\alpha\cos\left(\frac{\pi}{2}\alpha\right)$	$\mu_\alpha\omega^\alpha\sin\left(\frac{\pi}{2}\alpha\right)$
Fractional Voigt	$\mu_0+\mu_\alpha\omega^\alpha\cos\left(\frac{\pi}{2}\alpha\right)$	$\mu_\alpha\omega^\alpha\sin\left(\frac{\pi}{2}\alpha\right)$

characterized by a single element, comprised of two constants whose behavior lies between Hookean solid and Newtonian fluid, has been investigated in recent studies (Royston et al., 2011, 2003). Their relative merits for characterizing the material viscoelasticity in USWE have not been investigated.

In this study, Voigt, Maxwell, standard linear solid (SLS), spring-pot (SP), and fractional Voigt (FV) models were compared through analytical and experimental studies in USWE. Analytical study was performed via prescribing shear elasticity and varying shear viscosity in Voigt models to calculate shear wave speeds at different excitation frequencies. The frequency-dependent shear wave speeds were used to optimize the parameters associated with different viscoelastic models via minimizing the difference between the predefined and predicted values of shear wave speed. The experimental study was conducted on a tissue-mimicking phantom. A mechanical shaker was used to generate a harmonic vibration at different excitation frequencies on the phantom and the resulting shear wave speed was measured via ultrasound transducer. The parameters associated with different viscoelastic models for the phantom was identified via least-square regression analysis.

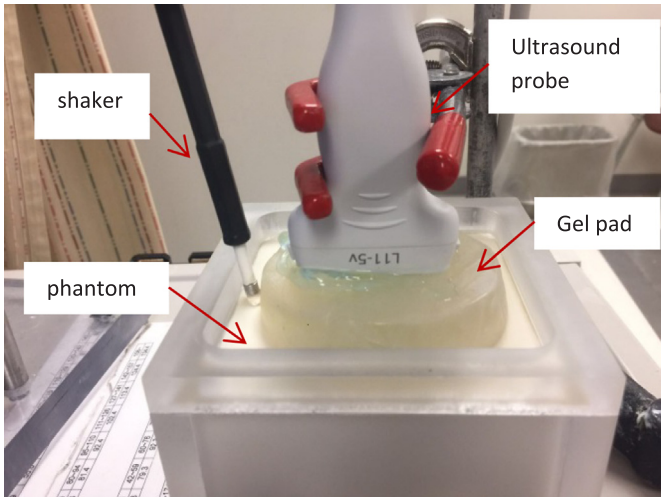

Fig. 3. Experimental setup of the USWE system. The shaker was in touch with the phantom to generate 0.1 s harmonic vibration while an ultrasound probe was placed on the gel pad, which was on the phantom to measure the shear wave speed of the phantom noninvasively.

2. Materials and methods

2.1. Forward problem

Frequency-dependent shear wave speed in USWE results from a complex shear modulus (μ) that can be expressed in the frequency domain by its real (storage, μ_R) and imaginary (loss, μ_I) parts of the shear modulus as (Royston et al., 2011),

$$\mu(\omega) = \mu_R(\omega) + i\mu_I(\omega) \quad (1)$$

The shear wave speed of a viscoelastic material is expressed as

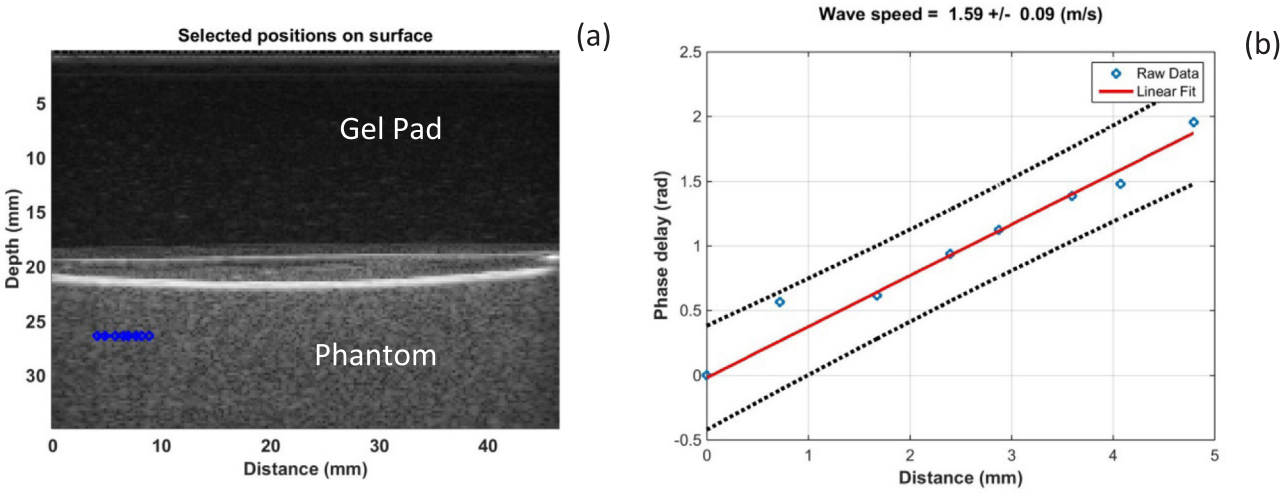

Fig. 4. (a) Representative B-mode image of the phantom. Eight locations in the phantom were selected to measure the shear wave speed of the phantom by using the ultrasound tracking beam. Blue points indicate points selected for measurement. (b) Representative Phase delay - distance relationship of the phantom at excitation frequency of 100 Hz. The wave phase change with position, in response to 0.1 s excitation was used to measure the shear wave speed.

$$c_{shear} = \sqrt{\frac{2}{\rho}\frac{\mu_R^2 + \mu_I^2}{\mu_R + \sqrt{\mu_R^2 + \mu_I^2}}} \quad (2)$$

Consider a half space of a linear viscoelastic isotropic material with density ρ = 1000 kg/m^3 and surface wave excitation is initiated via an indenter over the frequency range of 100–300 Hz at intervals of 50 Hz. Using a Voigt model to prescribe $\mu_R = \mu_0$ and $\mu_I = \omega\eta$, shear wave speed at different frequencies can be calculated. η is the shear viscosity. Additionally, corresponding ratios of storage to loss modulus ($\frac{\mu_R}{\mu_I}$) at different excitation frequencies were calculated (Fig. 1). For the analytical study, the following material parameters were used: μ_0 = 2 kPa, η ranges from 2 to 6.5 Pa s at an interval of 0.5 Pa s. These material parameters are comparable to those of soft biological tissue.

2.2. Inverse problem

Shear wave speeds obtained from the forward problem were fit with Voigt, Maxwell, SLS, spring-pot, and FV models of viscoelasticity to estimate material parameters over the whole frequency range of interest (Fig. 2). Parameters associated with different viscoelastic models were used to calculate storage modulus μ_R,loss modulus μ_I (Table 1).

Storage and loss moduli were then used to predict shear wave speed. Given the predefined shear wave speeds at different frequencies, the material parameters for the five viscoelastic models were identified by using the Levenberg-Marquardt nonlinear, least-square algorithm for minimizing the objective function which reflects the agreement between predefined and predicted shear wave speeds at different excitation frequencies, which yields unique estimates of the material parameters (Suh and Bai, 1998; Zhou et al., 2016). Residual error is the output of the objective function, Ω= $\sum_{n=1}^{N}(c_n^T - c_n^E)^2$, where the superscript E and T refer to the experimentally measured and theoretically calculated values of shear wave speed, and subscript n indicates a particular experimental state. The ranges over which parameter values were sought were identical with limiting values based on the physical meaning of each parameter. Multiple iterations of functional minimization were performed to ensure that the obtained parameter values were insensitive to the initial guesses within the prescribed ranges.

2.3. Experiments on phantom

USWE experiments were conducted on a tissue-mimicking phantom (CIRS Inc, Norfolk, Virginia). Shear wave propagation in the tissue mimicking phantom was measured by the USWE. A sinusoidal vibration signal was generated by a function generator (Model 33120 A, Agilent, Santa Clara, CA). The vibration signals were generated at five frequencies from 100 Hz to 300 Hz at increments of 50 Hz (Kubo et al., 2018). The excitation signal at a frequency was amplified by an audio amplifier (Model D150A, Crown Audio Inc., Elkhart, IN) and then drove an electromagnetic shaker (Model: FG-142, Labworks Inc., Costa Mesa, CA 92626). The shaker applied a 0.1 s harmonic vibration on the surface of the phantom using an indenter with 3 mm diameter. The propagation of the shear wave in the phantom was measured using a linear array transducer (L11-5v, Philips Healthcare, Andover, MA) transmitting at 6.4 MHz center frequency on the acoustic standoff pad (Fig. 3). The acoustic standoff pad was placed on the phantom increasing the distance between the phantom and transducer to improve ultrasound imaging quality. The transducer was connected to the ultrasound system (Vantage 1, Verasonics Inc, Kirkland, WA).

Detection of phantom motion is guided by ultrasound imaging. The phantom motion at a given location can be analyzed by cross-correlation analysis of the ultrasound tracking beam. In this study, eight locations over a length of approximately 8 mm were selected to measure the phantom motion (Fig. 4a.). A high frame rate of 2000 frame/s is used to detect phantom motion in response to the vibration excitation at 100, 150, 200, 250 and 300 Hz. The wave phase delay over the eight locations is presented in Fig. 4b. The wave speed was analyzed by the change in wave phase with distance. Using the phantom motion at the first location as a reference, the wave speed was measured using the wave phase delay of the remaining locations relative to the first location. At each frequency, the wave speed in the phantom was estimated using a phase gradient method.

$$c_s(f) = 2\pi f\frac{\Delta r}{\Delta\varphi} \quad (3)$$

where Δr is the distance between 2 detected locations and $\Delta\varphi$ is the phase change over that distance, f is the excitation frequency in Hz. The regression of phase change with distance is analyzed and the wave speed is measured with a 95% confidence interval in the format of mean ± standard error. Repetitive measurements were performed. Small standard deviation shows measurements were good.

3. Results

Results of the best fits in terms of shear wave speed – excitation frequency relationship using five viscoelastic models and associated parameters in the analytical study are provided in Fig. 5. Residual

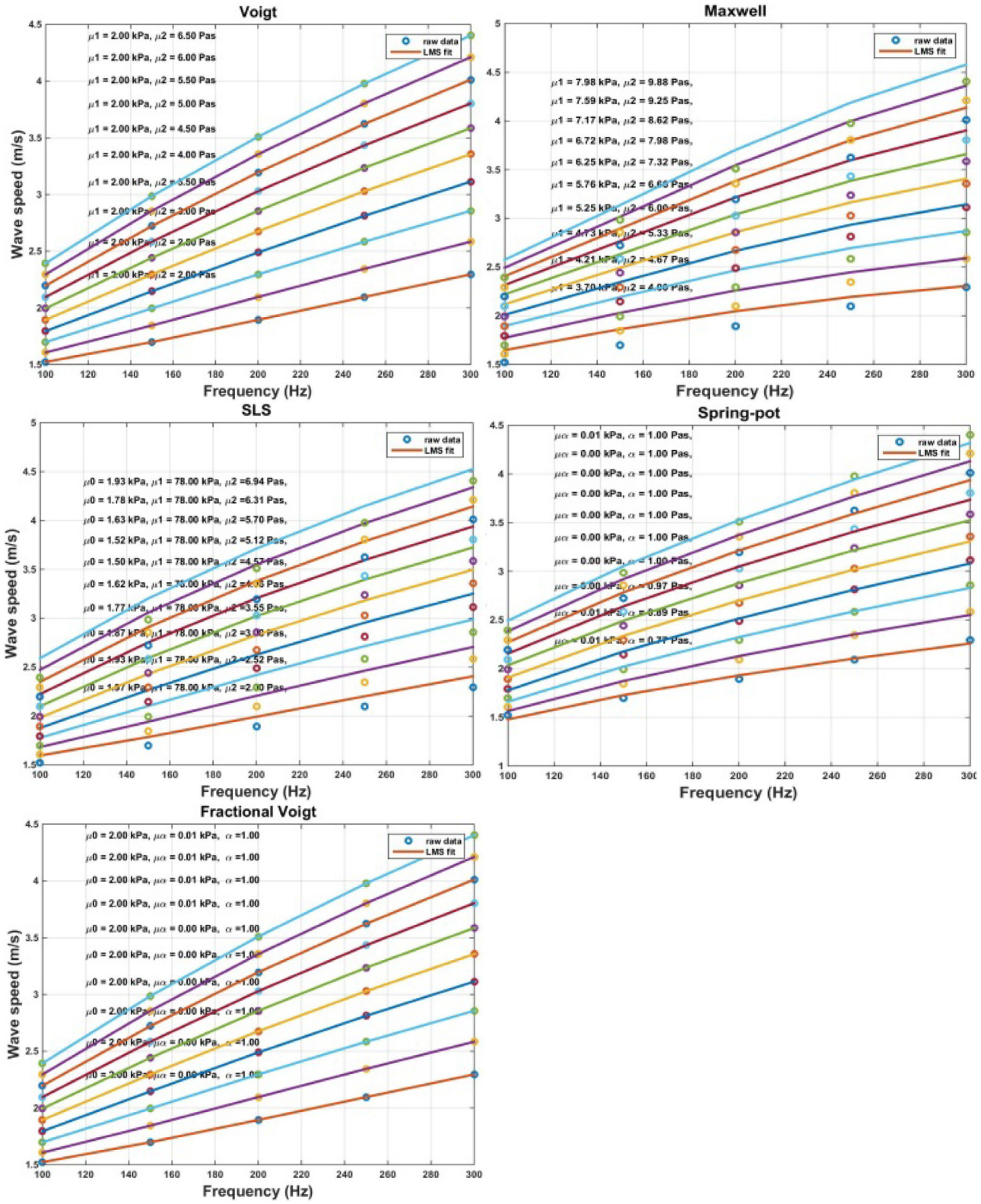

Fig. 5. Best fit Voigt, Maxwell, SLS, spring-pot, and FV models based on surface wave speed-frequency relationships. '$_{o}$' raw data;'– ', estimated values based on viscoelastic model.

errors of five viscoelastic models are provided in Table 2. It is seen that agreement is good with Voigt, spring-pot, and FV models; yet large discrepancies are seen with Maxwell and SLS models. Best fit in terms of ratio of storage to loss modulus as a function of excitation frequency for different viscoelastic models in the analytical study was provided in Fig. 6. It shows that integer and FV models fit well while large discrepancies were seen with Maxwell, SLS, and spring-pot models.

Voigt, Maxwell, SLS, spring-pot, and the fractional order Voigt models for viscoelasticity were used to fit the experimental data. Results of the best fit in terms of shear wave speed – excitation

Table 2
Residual error of the viscoelastic models in analytical studies.

Model	Voigt	Maxwell	SLS	Spring-pot	Fractional Voigt
Residual error	1.406e-20	0.0058	0.1797	0.0233	6.72e-13

frequency relationship and associated identified parameters using different viscoelastic models are provided in Fig. 7. Residual errors of different viscoelastic models are shown in Table 3. Referring to Table 3, it is seen that integer and FV models generally outperform other models. Table 4 shows the calculated ratio of storage to loss modulus of the phantom for different viscoelastic models at various excitation frequencies. It showed that this ratio increased with frequency for the Maxwell model; this ratio is a constant for spring-pot model and close to zero; for the Voigt, SLS, and FV models, this ratio decreased with frequency.

4. Discussions

The aim of this study was to evaluate different viscoelastic models for characterizing the dynamic behavior of soft tissue in terms of shear wave speeds; excitation frequency and ratio of storage to loss modulus; and excitation frequency in the USWE. The shear wave speed at different excitation frequencies in the analytical study was theoretically predefined and fitted with different viscoelastic models. In the experimental study, a shaker was used to generate a harmonic mechanical vibration on the surface of the phantom at five frequencies (100, 150, 200, 250 and 300 Hz). The resulting wave propagation in the phantom was noninvasively measured using an ultrasound technique. The magnitude of wave motion increased with excitation frequency. The wave length is inversely proportional to the wave frequency while attenuation rises with the wave frequency. The range of the excitation frequency in this study was selected based on wave motion amplitude, spatial resolution, and wave attenuation. While quantitative results obtained in the tissue-mimicking phantom may not reflect soft biological tissues, we expect that the observed effect of different viscoelastic models will be retained for soft biological tissues.

Obtained data are in agreement with the published literature. The dynamic response of the tissue phantom in terms of wave speed dispersion with frequency is qualitatively similar to that of soft biological tissues (Dai et al., 2014). The wave speed values of the phantom obtained in this paper are in the same range as reported in references (Kirkpatrick et al., 2004; Potts et al., 1983). The shear elasticity and viscosity of human skin was reported by the surface wave technique ranging from 5.67 kPa to 33 kPa and from 3.86 Pas to 26.26 Pas (Boyer et al., 2007; Xiaoming Zhang, 2017; Zhang, 2011; Zhang et al., 2017a). The value obtained on the phantom falls in the range of that literature.

Shear wave speed dispersion derived from the elastography technique has been used to estimate the shear viscoelasticity with an assumed viscoelastic model type. For both the analytical and experimental studies, it showed that Voigt and fractional Voigt outperform other models in characterizing the dynamic behavior of material. Moreover, $\frac{\mu_R}{\mu_I}$, which is an indicator of attenuation per cycle, has been proven to be a valid measure of material viscoelasticity (von Gierke et al., 1952). It is well known that attenuation in USWE increases with excitation frequency for soft tissue. For the Maxwell and SLS model, the loss modulus decreases with frequency so it results in large discrepancies in both shear wave speed and $\frac{\mu_R}{\mu_I}$ in USWE. For the spring-pot model, $\frac{\mu_R}{\mu_I} = \tan\left(\frac{\pi}{2}\alpha\right)$ is only dependent on α, irrespective of excitation frequency, resulting in large discrepancy in $\frac{\mu_R}{\mu_I}$. Integer and fractional order Voigt models yield a loss modulus which increases linearly with frequency and increases with the power of frequency where $\alpha < 1$, respectively. Loss modulus correlates with attenuation of wave motion; attenuation increase with excitation frequency which is valid in USWE. The model can be identified from $\frac{\mu_R}{\mu_I}$ versus frequency even though different models lead to nearly the same fitting. Comparison of estimates of $\frac{\mu_R}{\mu_I}$ is more clearly identifiable for which viscoelastic model type is more appropriate than comparing estimates of shear wave speed.

The various components of the soft biological tissue are grouped into 2 phases: a solid phase consisting of a collagenous extracellular matrix and cells and a fluid phase consisting of an inter-fibrillar fluid. The fluid viscosity varies depending on matrix density and structure. The solid matrix forms an ensemble of various size channels or pores through which fluid moves when the tissue is loaded. On the other hand, the solid matrix itself behaves viscoelastically, because of the numerous hydrogen-bonded cross links between matrix fibers. When $\alpha \rightarrow 0$, the fractional unit behaves like a Hookean spring; when $\alpha \rightarrow 1$, it behaves as a Newtonian dashpot. For intermediate values of α, it behaves as a viscoelastic material. A fractional order Voigt model represents multiscale rate-dependent stress-strain interactions in soft biological tissues. Another advantage of the fractional Voigt model is its attribute that the temporal response takes on characteristics of power-law behavior, which has been observed in a number of biological materials (Coussot et al., 2009; Kiss et al., 2004). This model can be used to obtain specific parameters associated with disease and treatment and be able to predict underlying remodeling in tissue with pathology.

We use USWE for skin related disease such as scleroderma. Skin is a tissue does not involve deformation so we did not discuss the effect of deformation on the shear wave speed. For other soft tissues, such as lung, we should definitely take the deformation into account. It has been shown that acoustic properties of material are altered with deformation and pressurization, correspondingly changing the wave propagation speed or reflected wave amplitude in the material (Galich and Rudykh, 2015; Kobayashi and Vanderby, 2007; Zhou et al., 2017). Numerous studies have shown the relationship between the echo intensity and the stress or strain experienced by the isolated soft tissues under static or cyclic loading scenarios (Duenwald et al., 2011; Pan et al., 1998).

A range of viscoelastic constitutive models have been proposed to interpret shear wave measurements. These models attempt to relate measurable phenomena to the underlying elasticity and damping of the material, both of which are typically rate- (frequency-) dependent. These viscoelastic models often manifested as complex shear modulus with the real part as the storage modulus and imaginary part as the loss modulus. The ultrasound shear wave elastography can be used to determine the parameters associated with the viscoelastic model if their storage and loss modulus are known.

In this study, the viscoelastic models were evaluated in terms of dynamical response of the material manifested as shear wave speed at different vibration frequencies. Once the material parameters associated with the viscoelastic models are identified, they can be further validated via predicting the quasi-static stress-strain response of the material in the stress relaxation test and comparing the results with the experimentally measured response of the material.

Several limitations should be taken into account. These models assume the material is homogeneous; in fact, the skin is a heterogeneous material with each layer of different mechanical properties. In the future, layer-specific viscoelastic models will be developed to investigate deeper tissues within the skin. Secondly, these models assume the viscoelastic properties are independent of temperature. It has been shown that temperature plays a critical role in the mechanical properties of skin (Zhang, 2011). Wave speed and wave amplitude decay rate are higher at room temperature than those at body temperature indicating a difference of tissue viscoelastic properties at room temperature and body temperature. Future studies will incorporate temperature into modelling the viscoelasticity of skin in USWE.

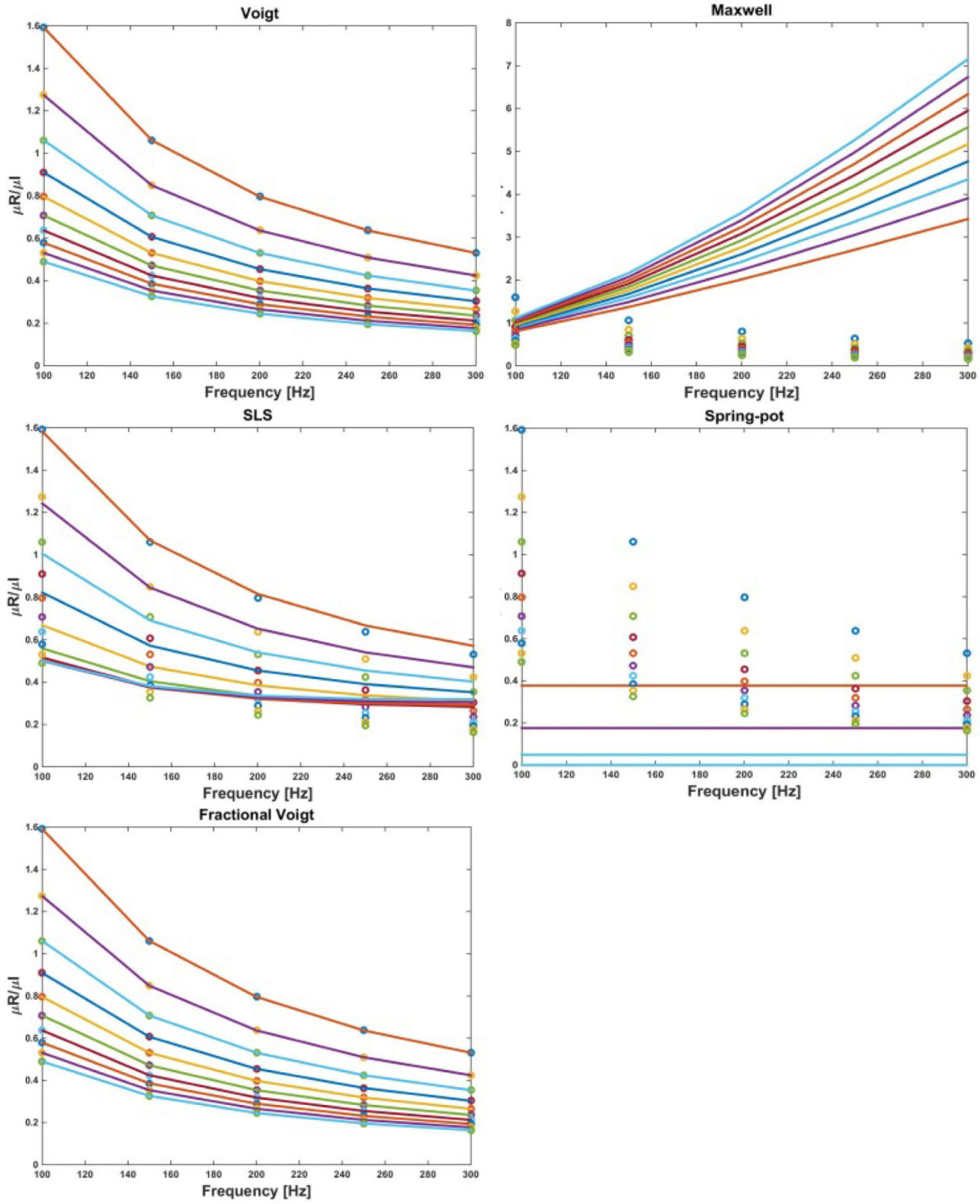

Fig. 6. Best fit Voigt, Maxwell, SLS, spring-pot, and FV models based on ratio of storage to loss modulus- excitation frequency relationships.'$_{o}$' raw data; '–', estimated values based on viscoelastic model.

5. Conclusion

In this study, five viscoelastic models (Voigt, Maxwell, SLS, spring-pot, and FV) are compared analytically and experimentally for USWE. The frequency-dependent shear wave speed was measured experimentally from 100 to 300 Hz by applying mechanical vibration on the phantom. Shear wave speed and ratio of storage to loss modulus as a function of excitation frequency both from the analytical and experimental studies suggest that the FV model can characterize the viscoelastic behavior of soft tissue. Quantifying the dynamic behavior of

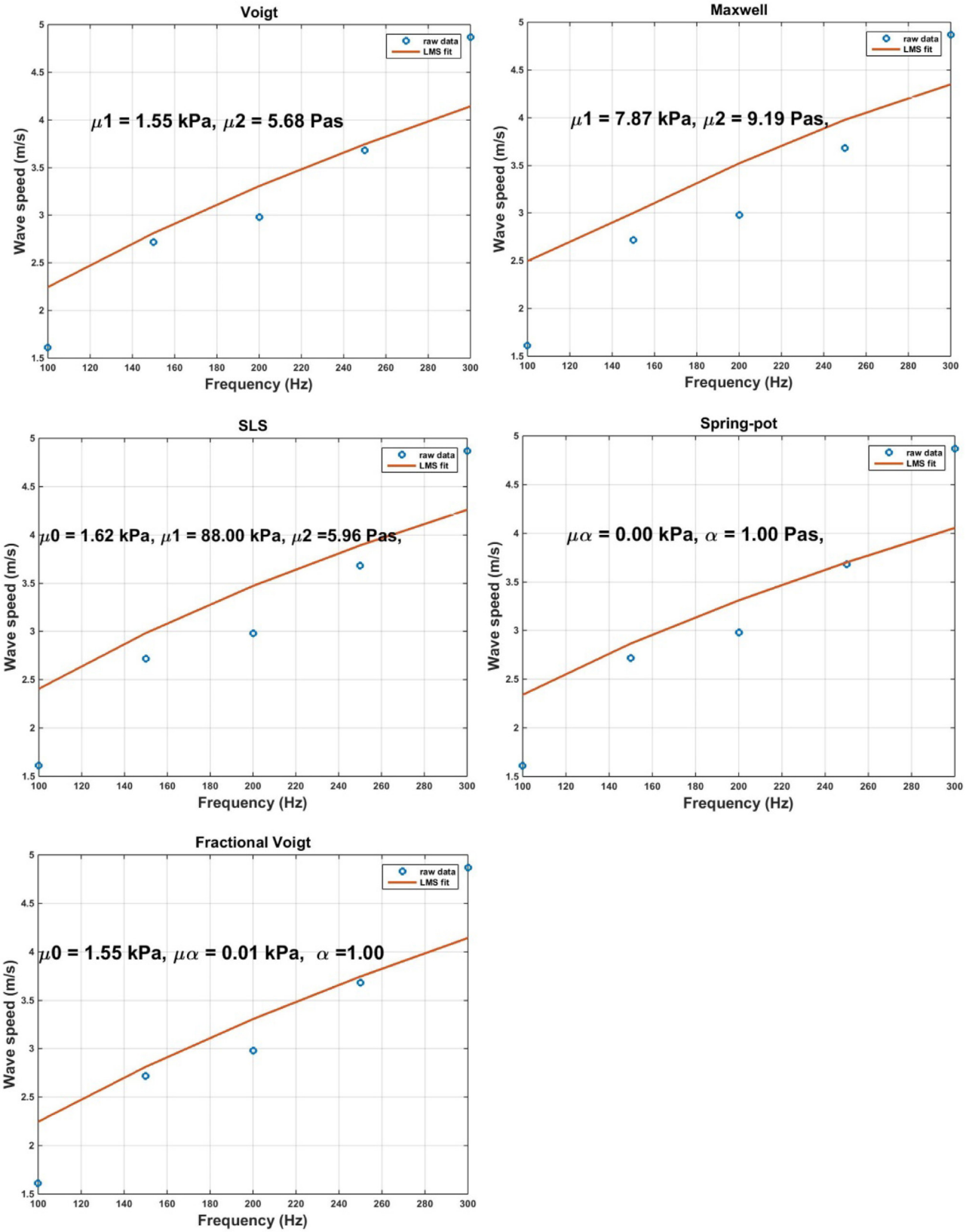

Fig. 7. Best fit Voigt, Maxwell, SLS, spring-pot, and FV models based on surface wave speed-frequency relationships. '$_{o}$' raw data; '–', estimated values based on viscoelastic model.

Table 3
Residual error of the viscoelastic models in experimental studies.

Model	Voigt	Maxwell	SLS	Spring-pot	Fractional Voigt
Residual error	1.0569	1.2911	1.2501	1.3305	1.0529

Table 4
$\frac{\mu_R}{\mu_I}$ of the viscoelastic models at different excitation frequencies in the experimental studies.

	Frequency [Hz]				
$\frac{\mu_R}{\mu_I}$	**100**	**150**	**200**	**250**	**300**
Voigt	0.43	0.29	0.22	0.17	0.14
Maxwell	1.01	1.93	3.15	4.63	6.27
SLS	0.48	0.35	0.3	0.28	0.27
Spring-pot	3.62e-14	3.62e-14	3.62e-14	3.62e-14	3.62e-14
Fractional Voigt	0.43	0.29	0.22	0.17	0.14

soft tissue in USWE is a necessary step to understand physiological and pathological conditions. The FV model may provide a more robust and accurate model for wave propagation in soft biological tissues over a wider range of excitation frequencies.

Acknowledgements

This study is supported by National Institute of Health (NIH) R01HL125234 from the National Heart, Lung and Blood Institute. We thank Mrs. Jennifer Poston for editing this manuscript.

References

Asbach, P., Klatt, D., Schlosser, B., Biermer, M., Muche, M., Rieger, A., Loddenkemper, C., Somasundaram, R., Berg, T., Hamm, B., 2010. Viscoelasticity-based staging of hepatic fibrosis with multifrequency MR elastography. Radiology 257, 80–86.

Boyer, G., Zahouani, H., Le Bot, A., Laquieze, L., 2007. In vivo characterization of viscoelastic properties of human skin using dynamic micro-indentation, Engineering in Medicine and Biology Society, 2007. EMBS 2007. In: Proceedings of the 29th Annual International Conference of the IEEE. IEEE, pp. 4584–4587.

Cheng, Y.-S., Zhou, B., Kubo, K., An, K.-N., Moran, S.L., Amadio, P.C., Zhang, X., Zhao, C., 2018. Comparison of two ways of altering carpal tunnel pressure with ultrasound surface wave elastography. J. Biomech.

Clements, P., Lachenbruch, P., Siebold, J., White, B., Weiner, S., Martin, R., Weinstein, A., Weisman, M., Mayes, M., Collier, D., et al., 1995. Inter and intraobserver variability of total skin thickness score (modified Rodnan TSS) in systemic sclerosis. J. Rheumatol. 22, 1281–1285.

Coussot, C., Kalyanam, S., Yapp, R., Insana, M.F., 2009. Fractional derivative models for ultrasonic characterization of polymer and breast tissue viscoelasticity. IEEE Trans. Ultrason. Ferroelectr. Freq. Control 56.

Dai, Z., Peng, Y., Mansy, H.A., Sandler, R.H., Royston, T.J., 2014. Comparison of poroviscoelastic models for sound and vibration in the lungs. J. Vib. Acoust. 136, 050905.

Duenwald, S., Kobayashi, H., Frisch, K., Lakes, R., Vanderby, R., 2011. Ultrasound echo is related to stress and strain in tendon. J. Biomech. 44, 424–429.

Galich, P.I., Rudykh, S., 2015. Influence of stiffening on elastic wave propagation in extremely deformed soft matter: from nearly incompressible to auxetic materials. Extrem. Mech. Lett. 4, 156–161.

Kirkpatrick, S.J., Duncan, D.D., Fang, L., 2004. Low-frequency surface wave propagation and the viscoelastic behavior of porcine skin. J. Biomed. Opt. 9, 1311–1320.

Kiss, M.Z., Varghese, T., Hall, T.J., 2004. Viscoelastic characterization of in vitro canine tissue. Phys. Med. Biol. 49, 4207.

Kobayashi, H., Vanderby, R., 2007. Acoustoelastic analysis of reflected waves in nearly incompressible, hyper-elastic materials: forward and inverse problems. J. Acoust. Soc. Am. 121, 879–887.

Kubo, K., Cheng, Y.-.S., Zhou, B., An, K.-.N., Moran, S.L., Amadio, P.C., Zhang, X., Zhao, C., 2018. The quantitative evaluation of the relationship between the forces applied to the palm and carpal tunnel pressure. J. Biomech.

Kubo, K., Zhou, B., Cheng, Y.S., Yang, T.H., Qiang, B., An, K.N., Moran, S.L., Amadio, P.C., Zhang, X., Zhao, C., 2017. Ultrasound elastography for carpal tunnel pressure measurement: a cadaveric validation study. J. Orthop. Res. Off. Publ. Orthop. Res. Soc.

Leng, X., Zhou, B., Deng, X., Davis, L., Lessner, S.M., Sutton, M.A., Shazly, T., 2018. Experimental and numerical studies of two arterial wall delamination modes. J. Mech. Behav. Biomed. Mater.

Osborn, T., Zhang, X., Kalra, S., Zhou, B., Bartholmai, B., 2017. A Non-Invasive Ultrasound Surface Wave Elastography Technique for Assessing Interstitial Lung Disease, ARTHRITIS & RHEUMATOLOGY. WILEY 111 RIVER ST, HOBOKEN 07030-5774, NJ USA.

Pan, L., Zan, L., Foster, F.S., 1998. Ultrasonic and viscoelastic properties of skin under transverse mechanical stress in vitro. Ultrasound Med. Biol. 24, 995–1007.

Potts, R.O., Chrisman Jr, D.A., Buras Jr, E.M., 1983. The dynamic mechanical properties of human skin in vivo. J. Biomech. 16, 365–372.

Prim, D.A., Zhou, B., Hartstone-Rose, A., Uline, M.J., Shazly, T., Eberth, J.F., 2016. A mechanical argument for the differential performance of coronary artery grafts. J. Mech. Behav. Biomed. Mater. 54, 93–105.

Royston, T.J., Dai, Z., Chaunsali, R., Liu, Y., Peng, Y., Magin, R.L., 2011. Estimating material viscoelastic properties based on surface wave measurements: a comparison of techniques and modeling assumptions. J. Acoust. Soc. Am. 130, 4126–4138.

Royston, T.J., Yazicioglu, Y., Loth, F., 2003. Surface response of a viscoelastic medium to subsurface acoustic sources with application to medical diagnosis. J. Acoust. Soc. Am. 113, 1109–1121.

Shazly, T., Rachev, A., Lessner, S., Argraves, W.S., Ferdous, J., Zhou, B., Moreira, A.M., Sutton, M., 2015. On the uniaxial ring test of tissue engineered constructs. Exp. Mech. 55, 41–51.

Suh, J.-K., Bai, S., 1998. Finite element formulation of biphasic poroviscoelastic model for articular cartilage. J. Biomech. Eng. 120, 195–201.

von Gierke, H.E., Oestreicher, H.L., Franke, E.K., Parrack, H.O., von Wittern, W.W., 1952. Physics of vibrations in living tissues. J. Appl. Physiol. 4, 886–900.

Xiaoming Zhang, B.Z., Kalra, Sanjay, Bartholmai, Brian, Greenleaf, James, Osborn, Thomas, 2017. Quantitative assessment of scleroderma using ultrasound surface wave elastography, In: Proceedings of the IEEE International Ultrasonics Symposium (IUS), 2017, pp. 1–3.

Zhang, X., Osborn, T., Zhou, B., Bartholmai, B., Greenleaf, J.F., Kalra, S., 2017a. An ultrasound surface wave elastography technique for noninvasive measurement of surface lung tissue. J. Acoust. Soc. Am. 141 (3721-3721).

Zhang, X., Osborn, T., Zhou, B., Meixner, D., Kinnick, R., Bartholmai, B., Greenleaf, J., Kalra, S., 2017b. Lung ultrasound surface wave elastography: a pilot clinical study. IEEE Trans. Ultrason. Ferroelectr. Freq. Control 64, 1298–1304.

Zhang, X., Osborn, T.G., Pittelkow, M.R., Qiang, Kinnick, R.R., Greenleaf, J.F., 2011. Quantitative assessment of scleroderma by surface wave technique. Med. Eng. Phys. 33, 31–37.

Zhang, X., Zhou, B., Kalra, S., Bartholmai, B., Greenleaf, J., Osborn, T., 2018a. An ultrasound surface wave technique for Assessing skin and lung diseases. Ultrasound Med. Biol. 44, 321–331.

Zhang, X., Zhou, B., Miranda, A., Trost, L.W., 2018b. A novel non-invasive ultrasound vibro-elastography technique for assessing patients with erectile dysfunction and peyronie's disease. Urology.

Zhou, B., Alshareef, M., Prim, D., Collins, M., Kempner, M., Hartstone-Rose, A., Eberth, J.F., Rachev, A., Shazly, T., 2016. The perivascular environment along the vertebral artery governs segment-specific structural and mechanical properties. Acta Biomater. 45, 286–295.

Zhou, B., Sit, A.J., Zhang, X., 2017. Noninvasive measurement of wave speed of porcine cornea in ex vivo porcine eyes for various intraocular pressures. Ultrasonics 81, 86–92.